Proof Delivery Form
Please return this form with your proof

CUP reference: FM – 12,805

Date of delivery:

Journal and Article number: FLM 324

Volume and Issue Number: 000(0)

Colour Figures: Nil

Number of pages in the proof: 25

Author queries:

Typesetter queries:

Non-printed material:

CAMBRIDGE
UNIVERSITY PRESS

offprint order form
(to be returned with the corrected proofs)

Journal of Fluid Mechanics   *volume……… no………*

Offprints

50 offprints of each article will be supplied free. Additional offprints may be purchased at the price show below. The total offprint order will be sent by surface mail within one month of publication to the address given below.

Number of offprints required in addition to the 50 free copies

Offprints to be sent to (PRINT IN BLOCK CAPITALS) ....
....
.... Post/Zip Code.................
Date......................................Author(s)..
Article title...

All enquiries about offprints should be addressed to the printer:
Journals Office, Cambridge University Press, University Printing House, Shaftesbury Road, Cambridge. CB2 2BS UK

Charges for extra offprints (excluding VAT)

Number of copies	25	50	100	150	200	per 50 extra
1-4 pages	£20.50	£36.50	£55.50	£76.50	£98.50	£20.50
5-8 pages	£36.50	£52.50	£77.00	£103.00	£127.00	£36.50
9-16 pages	£38.50	£57.50	£91.50	£122.50	£157.00	£38.50
17-24 pages	£41.50	£64.50	£105.50	£147.00	£192.50	£41.50
extra 8 pages	£7.00	£9.00	£15.50	£26.50	£32.00	£7.00

Methods of payment

VAT at the local rate may he <u>added</u> to the above charges if paid by EU residents not registered for VAT.
If registered, please quote your VAT number, or the VAT number of any agency paying on
your behalf if it is registered

❑Payment against invoice. The invoice will be sent to you after publication of your article.
❑Cheques should be made out to Cambridge University Press.

❑Payment by someone else. Please enclose the official order when returning this form. Or ensure that when the order is sent, it mentions the name of the journal and the article title.
❑Payment may be made by any credit card bearing the Interbank Symbol.

Signature of card holder .... Amount.....................
Card number....................................Card expiry date............................
Card verification number...........................
The card verification number is a 3 digit number printed on the **back** of your **Visa** or **Master card**, it appears after and to the right of your card number. For **American Express** the verification number is 4 digits, and printed on the **front** of your card, after and to the right of your card number.
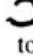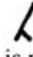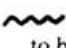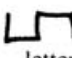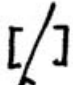
Please advise if address registered with card company is different from above

For office use only

Reference   Sent   Acknowledged   Price   Received

Proof correction symbols

Correction required	Marginal mark	Corresponding mark in text
Insert new material	Inserted material, followed by caret,	
Delete		(Cross out what is not wanted)
Substitute new material for something typeset	Write new material followed by	(Cross out material to be replaced)
Leave as printed	*stet*	..... under material to remain
Insert space	#/	where space is required
Take out space (close up)		around material to be closed up
Insert hyphen		where hyphen is required
Change letter(s) to capital(s)	*cap*	under letter(s) required
Change letter(s) to small capital(s)	*sm. cap*	under letter(s) required
Change to small letter(s)	*l.c.*	(Encircle required letter(s))
Change to bold type	*bold*	under letter(s) to be altered
Change to italic type	*itals*	under letter(s) to be altered
Begin a new paragraph	*NP*	before first word of new paragraph

Correction required	Marginal mark	Corresponding mark in text
No new paragraph	*run on*	between paragraphs
Inferior (subscript) letter, e.g. x		if to be inserted; cross out incorrect letter if a replacement
Superior (superscript) letter, e.g. p		if to be inserted; cross out incorrect letter if a replacement
Transpose letters or words	*trs*	between letters or words
Indicate letters set upside-down		(Encircle letters to be altered)
Broken letter; replace by similar but undamaged character	X	(Encircle letters to be altered)
Insert parentheses		where parentheses required
Insert square brackets		where square brackets required
Insert apostrophe		where apostrophe required
Insert quotation marks		where quotation marks required

CAMBRIDGE UNIVERSITY PRESS

transfer of copyright

Please read the notes overleaf and then complete, sign, and return one copy of this form with the corrected proof, or as soon as possible thereafter to the **Journal of Fluid Mechanics, Department of Applied Mathematics and Theoretical Physics, Centre for Mathematical Science, Wilberforce Road, Cambridge CB3 0WA, UK.**

JOURNAL OF FLUID MECHANICS

In consideration of the publication in **JOURNAL OF FLUID MECHANICS**

of the contribution entitled: ....

....

by (all authors' names): ....

....

1 To be filled in if copyright belongs to you
Transfer of copyright

I/we hereby assign to Cambridge University Press full copyright in all formats and media in the said contribution.

I/we warrant that I am/we are the sole owner or co-owners of the material and have full power to make this agreement, and that the material does not contain any defamatory matter or infringe any existing copyright.

I/we further warrant that permission has been obtained from the copyright holder for any material not in my/our copyright and the appropriate acknowledgement made to the original source. I/we attach copies of all permission correspondence.

I/we hereby assert my/our moral rights in accordance with the UK Copyrights Designs and Patents Act (1988).

Signed (tick one)   ❑   the sole author(s)

❑ one author authorised to execute this transfer on behalf of all the authors of the above article

Name (block letters) ....

Institution/Company ....

Signature: ....   Date: ....

(Additional authors should provide this information on a separate sheet.)

2 To be filled in if copyright does not belong to you
a   Name and address of copyright holder ....

....

....

b   The copyright holder hereby grants to Cambridge University Press the non-exclusive right to publish the contribution in the journal and to deal with requests from third parties in the manner specified in paragraphs 4 and 6 overleaf.

(Signature of copyright holder or authorised agent) ....

3 US Government exemption
I/we certify that the paper above was written in the course of employment by the United States Government so that no copyright exists.

Signature: ....   Name (Block letters): ....

4 Requests received by Cambridge University Press for permission to reprint this article should be sent to (see para. 5 overleaf)
Name and address (block letters) ....

....

Notes for contributors

1 The information provided on this form will be held in perpetuity for record purposes. The name(s) and address(es) of the author(s) of the contribution may be reproduced in the journal and provided to print and online indexing and abstracting services and bibliographic databases.

2 The Journal's policy is to acquire copyright in all contributions. There are two reasons for this: *(a)* ownership of copyright by one central organisation tends to ensure maximum international protection against unauthorised use; *(b)* it also ensures that requests by third parties to reprint or reproduce a contribution, or part of it, are handled efficiently and in accordance with a general policy that is sensitive both to any relevant changes in international copyright legislation and to the general desirability of encouraging the dissemination of knowledge.

3 Two 'moral rights' were conferred on authors by the UK Copyright Act in 1988. In the UK an author's 'right of paternity', the right to be properly credited whenever the work is published (or performed or broadcast), requires that this right is asserted in writing.

4 Notwithstanding the assignment of copyright in their contribution, all contributors retain the following **non-transferable** rights:

- The right to (continue to) post a preprint of the contribution on their personal or departmental web page provided the first screen contains the statement that the paper has been accepted for publication in Journal of Fluid Mechanics published by Cambridge University Press together with the appropriate copyright notice. On publication the full bibliographical details (volume: issue number (date), page numbers) must be inserted after the journal title.
- Subject to file availability, the right to post the contribution as published on their own or their departmental home page provided the first screen includes full bibliographical details and the appropriate copyright notice.
- The right to make hard copies of the contribution or an adapted version for their own purposes, including the right to make multiple copies for course use by their students, provided no sale is involved.
- The right to reproduce the paper or an adapted version of it in any volume of which they are editor or author. Permission will automatically be given to the publisher of such a volume, subject to normal acknowledgement.

5 We shall use our best endeavours to ensure that any direct request we receive to reproduce your contribution, or a substantial part of it, in another publication (which may be an electronic publication) is approved by you before permission is given.

6 Cambridge University Press co-operates in various licensing schemes that allow material to be photocopied within agreed restraints (e.g. the CCC in the USA and the CLA in the UK). Any proceeds received from such licenses, together with any proceeds from sales of subsidiary rights in the Journal, directly support its continuing publication.

7 It is understood that in some cases copyright will be held by the contributor's employer. If so, Cambridge University Press requires non-exclusive permission to deal with requests from third parties, on the understanding that any requests it receives from third parties will be handled in accordance with paragraphs 4 and 5 above (note that your approval and not that of your employer will be sought for the proposed use).

8 Permission to include material not in your copyright
If your contribution includes textual or illustrative material not in your copyright and not covered by fair use / fair dealing, permission must be obtained from the relevant copyright owner (usually the publisher or via the publisher) for the non-exclusive right to reproduce the material worldwide in all forms and media, including electronic publication. The relevant permission correspondence should be attached to this form.

If you are in doubt about whether or not permission is required, please consult the Permissions Controller, Cambridge University Press, The Edinburgh Building, Shaftesbury Road, Cambridge CB2 2RU, UK. Fax: +44 (0)1223 315052. Email: lnicol@cambridge.org.

Please make a duplicate of this form for your own records

Subcritical instability on the attachment-line of an infinite swept wing

By T. K. S E N G U P T A AND A. D I P A N K A R

Department of Aerospace Engineering, IIT Kanpur 208 016, India

The leading-edge contamination (LEC) problem of an infinite swept wing is shown here as vortex-induced instability. The governing equation for receptivity is presented for LEC in terms of disturbance energy based on the Navier–Stokes equation. The unperturbed shear layer given by the swept Hiemenz boundary-layer solution is two-dimensional and an exact solution of incompressible the Navier–Stokes equation. Thus, the LEC problem is solved numerically by solving the full two-dimensional Navier–Stokes equation. The contamination at the attachment-line is shown by solving a receptivity to a convecting vortex moving outside the attachment-line boundary layer, which triggers subcritical spatio-temporal instability.

The mechanism of LEC is shown to be due essentially to a convecting counter-clockwise rotating vortex, whereas a clockwise rotating vortex displays much weaker receptivity. These results are consistent with experimental results for the bypass mechanism.

The role of linear and nonlinear mechanisms in the contamination problem is discussed as interactions between vorticity and velocity terms of the developed receptivity equation. The computed temporal growth rates reveal pattern formation during such instabilities. Proper orthogonal decomposition (POD) of the numerical solution shows the structure of the leading eigenvector as the coherent eddy excited during the bypass transition.

1. Introduction

The leading edge of a swept-back wing that is in contact with the fuselage is seen to experience abrupt transition due to the convection of continuous turbulent puffs along the attachment-line plane whenever the Reynolds number based on momentum thickness (Re_θ) is greater than 100 (or a Reynolds number based on displacement thickness, $Re_{\delta^*} = 245$), as observed by Poll (1979) and Arnal (1986); whereas various investigations based on linear and weakly nonlinear theories have shown the lowest critical Reynolds number as $Re_{\delta^*} = 535$, indicating the actual transition to be a subcritical mechanism. Hence, this problem continues to hold interest as seen by recent publications, see e.g. Theofilis *et al.* (2003), Obrist & Schmid (2003*a, b*) and Sengupta *et al.* (2004). A good introduction to leading-edge contamination (LEC) is provided in Theofilis *et al.* (2003) which summarizes that 'there exist two most significant unresolved issues in the stability of the attachment-line boundary layer.' The first relates to the issue of sub-critical instability and the second issue is that of relating the instability at the attachment-line to the events downstream, in the chordwise direction. It is natural to try to resolve the first issue and that is the principal motivation of the present study.

The experimentally observed value of the Reynolds number at transition by Poll (1979) and the critical Reynolds numbers obtained from linear and nonlinear stability analyses differ significantly. While the attachment-line boundary layer supports linear instability waves (shown by careful laboratory experiments in Pfenninger & Bacon 1969; Poll 1979; Arnal, Coustols & Jullien 1984; Hall, Malik & Poll 1984; Poll, Danks & Yardley 1996), they are not the cause of transition occurring at the attachment-line as no linear or weakly non-linear theory has related the two. The critical Reynolds number is reported as $Re_{\delta^*} = 583.1$ by Hall *et al.* (1984) – more than twice the experimental value – using a linear temporal stability analysis. Theofilis (1998) also reports the same critical Reynolds number based on a linear spatial analysis. Hall & Malik (1986) performed a weakly nonlinear analysis that showed a marginally lower threshold critical Reynolds number, $Re_{\delta^*} = 535$.

When a full incompressible Navier–Stokes equation was solved to reproduce experimentally observed LEC, there also appears to be no consensus. Spalart (1988)'s three-dimensional direct numerical simulation (DNS) spectral calculation could not produce the nonlinear equilibrium solution reported by Hall & Malik (1986), but it did produce the correct experimental transitional Reynolds number in Poll (1979). Spalart (1988) used white noise to trigger instability for spatial DNS, where spanwise periodicity and a buffer domain in the chordwise direction were used. Two-dimensional DNS results, however, produced conflicting results, with Theofilis (1998) predicting the wrong frequency of the disturbance as compared to the experimental value of Poll *et al.* (1996). Joslin (1995) reported the existence of the sub-critical two-dimensional equilibrium of Hall & Malik (1986). Subsequently, Joslin (1996) postulated that interactions of multiple three-dimensional modes lead to bypass transition. Joslin (1995) performed DNS without any periodicity assumption in the spanwise direction.

Theofilis *et al.* (2003) and Obrist & Schmid (2003*a,b*) have looked at three-dimensional mechanisms off the attachment-line plane. In Theofilis *et al.* (2003), the linear instability problem is revisited, whereas in Obrist & Schmid (2003*a*), the temporal stability problem is studied with estimates for the location of continuous spectrum and bounds for validity of linear approximation. In Obrist & Schmid (2003*b*), the potential of swept Hiemenz flow to support transiently growing non-normal modes has been investigated. Also, a numerical receptivity problem is solved to study the excitation of boundary-layer disturbances by free-stream vortices convected by the mean flow. The authors looked for non-modal solutions and the process is termed a *bypass transition*.

Theofilis *et al.* (2003) have noted that there exists a range of Reynolds numbers between 245 and 535, that remain unexplained by any weakly nonlinear theory. The authors noted that, 'a different physical mechanism is required to fill either this gap or that with linear theory', the larger gap of 245 and 583. Above-mentioned discrepancies prompted them to observe that, 'in order for further advances to be made in theory, new insight is necessary.' The present investigation is undertaken with this goal in mind. It should be noted that all the necessary ingredients for understanding are based on existing evidences of sub-critical instability in Sengupta, De & Sarkar (2003*a*, hereinafter referred to as SDS) for the Blasius boundary layer.

The mean flow field and coordinate systems for flow past a swept-back wing is schematically shown in figure 1. According to Arnal (1986), observed transition right at the leading edge cannot be explained by linear stability theory as 'the leading edge is contaminated by large turbulent structures coming from the wall at which the wing is fixed without resorting to linear process (bypass).' This is stated in Gaster (1965, 1967),
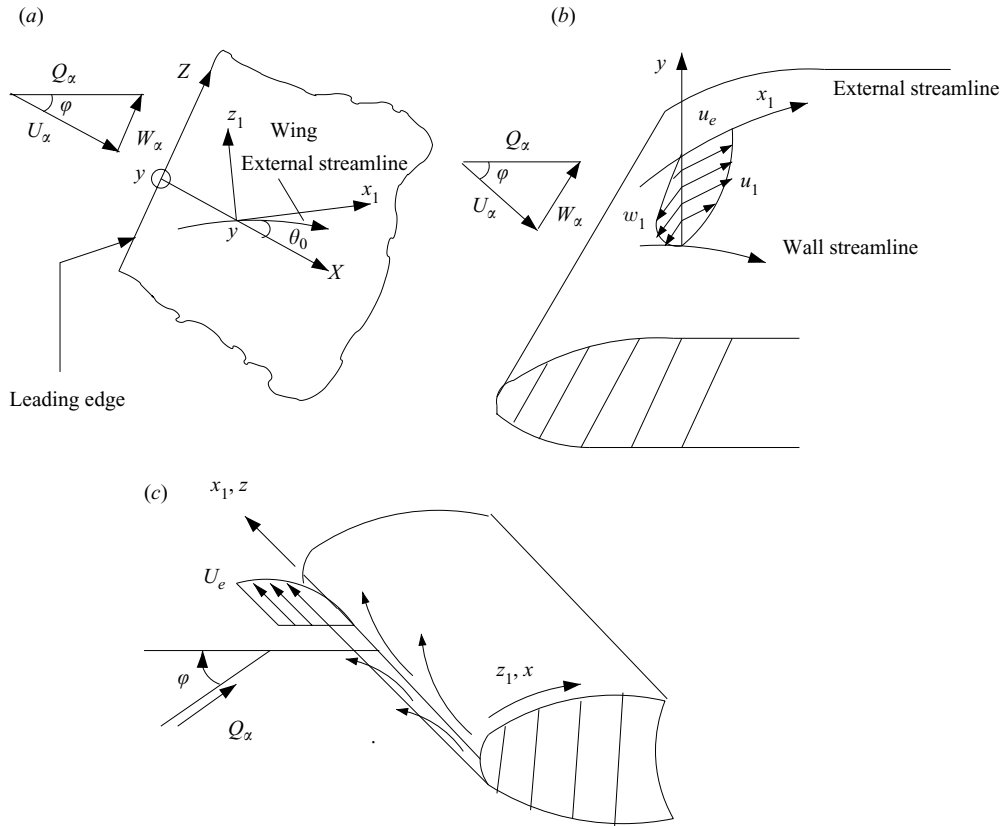
FIGURE 1. Flow profiles and schematic of co-ordinate systems for flow past a swept back wing. (*a*) Notation and coordinate system. (*b*) Streamwise (*u*) and cross-flow (*w*) mean velocity profiles. (*c*) Attachment line flow.

who tried to control LEC by decelerating the disturbances in the attachment-line plane. Gaster (1965) specifically noted that vortices associated with junction flow are fed in to the attachment-line boundary layer. On the attachment-line plane itself, the flow is essentially two-dimensional as established by Prandtl (1946), Cooke (1950) and Crabtree, Kuchemann & Sowerby (1963). In all early experiments (including the one by Poll 1979) the existence of *attachment-line vortical structure* is well established. It is, thus, natural to investigate the sub-critical instability by looking at the role of convecting vortical structures in explaining LEC from the solution of a two-dimensional Navier–Stokes equation in the attachment-line plane itself. Similar vortex-induced instability mechanism has been experimentally and theoretically established in SDS and Lim, Sengupta & Chattopadhyay (2004) for bypass transition of the Blasius boundary layer by a convecting vortex in the free stream.

Interaction between a convecting finite-core vortex and an underlying shear layer is important, as it relates to an unsteady flow separation process that was studied in Doligalski, Smith & Walker (1994) and Degani, Walker & Smith (1998). A later stage of transition that bypasses linear instability was studied by Brinckman & Walker (2001) in a quasi-two-dimensional framework. Basic ideas behind these studies have been discussed in SDS and are not repeated here. It is noted, however, that such interactions are present in (i) flow past surface-mounted obstacles; (ii) dynamic stall
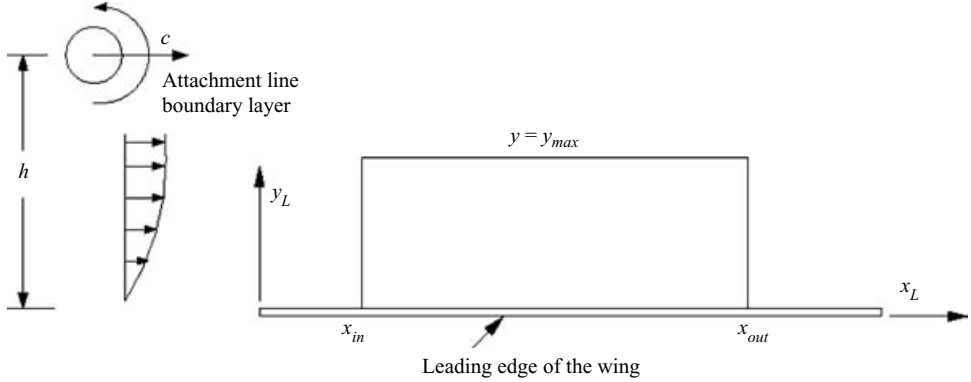
FIGURE 2. Schematic of the problem.

and blade vortex interaction; (iii) impulsive motion of bluff bodies; (iv) near-wall turbulence phenomenon associated with generation of hairpins – as discussed in Smith *et al.* (1991) and Robinson (1991).

A related model flow is studied in Obabko & Cassel (2002) where the convecting vortex is placed inside the shear layer and given a constant convection speed. In Sengupta, Lim & Chattopadhayay (2001) and SDS, coherent structures were created inside the boundary layer by a single convecting vortex that moved far above a steady boundary layer. In another set of studies, Peridier, Smith & Walker (1991*a*,*b*) considered a flow where a vortex placed above a plane wall without any mean convection caused the vortex to migrate and at the same time a thin unsteady boundary layer developed along the wall to satisfy the no-slip condition. For infinite strength of the vortex, impulsive start caused the unsteady boundary layer to thicken and recirculating eddies to develop owing to self-imposed adverse pressure gradient. Thus, the present study and those given in SDS and Sengupta *et al.* (2004) are qualitatively different where the coherent eddies are formed inside a steady boundary layer. In SDS and Lim *et al.* (2004), the receptivity mechanism was shown to be a strong function of strength, core size, sign and distance of the convecting vortex from the shear layer. In Sengupta *et al.* (2004), this model has been tested and computational results reported that show that sub-critical instability is triggered in the attachment-line boundary layer. In this paper, we discuss the mechanism of LEC with the help of the receptivity equation developed in SDS and provide various estimates of the ensuing spatio-temporal instability.

The schematic of the computational domain is shown in figure 2. Here, the vortex migrates outside the steady attachment-line boundary layer. In this model, the vortex mimics the turbulent structures created at the wing–body junction and is allowed to migrate at a constant height (h) over the attachment-line boundary layer with a constant speed c. The mechanism studied here is different to that in Obrist & Schmid (2003*b*) for a numerical receptivity experiment. First, they were looking for three-dimensional mechanisms and placed a pair of vortices symmetrically located on either side of the attachment-line plane. Secondly, the vortices were directed toward the wall, unlike the present case where the vortex moves parallel to the wall at a constant speed. Finally, the vortices in Obrist & Schmid (2003*b*) were constrained to move with the free-stream speed, while in Sengupta *et al.* (2004) and here, the vortex moves at different speeds and the results identify translational speeds for which receptivity is significant.

The attachment-line-boundary-layer solution is an exact solution of the Navier-Stokes equation and, as already noted, this creates a perfectly two-dimensional shear layer in the attachment-line plane. The computational domain chosen here is such that it can only suffer sub-critical instability. Sengupta *et al.* (2004) investigated eight cases for different parameters, indicating their relative importance. Here, a longer computational domain is used to trace the vortex-induced instability over longer distances and the physical mechanism behind LEC is explained. The coherent structures formed during the bypass transition are identified by a proper orthogonal decomposition (POD) technique proposed in Kosambi (1943) and discussed in detail in Holmes, Lumley & Berkooz (1996). A direct consequence of threading coherent structures with the statistical technique of POD provides a low-dimensional description of a fluid dynamical system, that is pursued here to provide a quantitative measure of the instability during LEC following the method of snapshots due to Sirovich (1987) and Rajaee, Karlsson & Sirovich (1994).

The paper is structured as follows. In the next section, the unperturbed flow field is briefly described. This provides the initial condition and the equilibrium solution whose instability is studied here. In §3, the formulation for the receptivity problem is re-stated. In §4, the numerical method used in solving the receptivity problem is briefly discussed. Results and discussion are provided in §5. The coherent structures arising out of bypass transition during LEC have been characterized by the POD technique in §6. In §7, formation of cellular structure for the time rate at which the energy sources and sinks change are discussed. Some concluding remarks are given in §8.

2. Unperturbed flow field

For the present exercise, the instability of the steady attachment-line boundary layer forming over the leading edge of an infinite swept wing or a yawed cylinder is studied. For this flow, Prandtl (1946) provided a simplified flow model in the vicinity of the attachment-line. If we consider z as the direction parallel to the generator of the body, then the assumption of infinite sweep is equivalent to neglecting all variations in the z-direction.

Cooke (1950) considered the boundary layer over an infinite-yawed wedge at zero angle of attack where, $U_e = U_m(x/L)^m$ and $W_e = const$.

The independent variable used is $\eta = \{(m + 1)U/2\nu x\}^{1/2}y$ and the corresponding dependent variables for the evaluation of the two components of velocity U and V in the (x, y)-plane are given by $\psi = (2U\nu x/(m + 1))^{1/2}f(\eta)$.

To solve this problem, Cooke extended the two-dimensional Falkner–Skan wedge solution by calculating the spanwise component of velocity in the layer separately via $w = Wg(\eta)$. The velocity profile obtained is the so-called Falkner–Skan–Cooke profile (see Arnal 1986). If we identify the (x_1, y_1, z_1) as the external streamline-fixed coordinate system (as shown in figure 1*a*), and if $U_1(y)$ and $W_1(y)$ are velocity components in this coordinate system, then

$$U_1(y) = U \cos\theta_0 + W \sin\theta_0,$$
$$W_1(y) = -U \sin\theta_0 + W \cos\theta_0.$$

Where θ_0 is the angle between the external streamline and the normal to the leading edge. Along the attachment-line, on the leading edge of an infinite swept wing the edge velocity is given by $U_e = kx$ and $W_e = W_\infty$. The attachment-line is depicted for the flow near the leading edge of a swept wing (with a sweep angle ϕ) in figure 1(*b*). In the

external streamline-fixed coordinate system, x_1 now coincides with the attachment-line and the attachment-line profile is obtained as, $U_1/U_{1e} = g$ and $W_1/U_{1e} = 0$, the details are available in Sengupta *et al.* (2004).

3. Formulation of the receptivity problem

The LEC problem is modelled here as a two-dimensional flow in the attachment-line plane excited by convecting vortices, as shown in figure 2. While in the actual flow, these vortices will be three-dimensional and they would move at non-uniform speed with varying height from the leading edge. A controlled scenario is studied here to understand the physical mechanism behind the observed phenomenon. To aid in understanding the mechanism, convecting turbulent structure is modelled as a two-dimensional vortex. The strength, sign and the speed of propagation are the parameters of the problem that were varied to investigate the receptivity mechanism in Sengupta *et al.* (2004) for the numerical investigation. The undisturbed flow is obtained as the solution of Falkner–Skan–Cooke equations. This is the initial condition used for the solution of the Navier-Stokes equation given by,

$$\nabla^2 \psi = -\omega, \tag{3.1}$$

$$\frac{\partial \omega}{\partial t} + \mathbf{V} \cdot \nabla \omega = \frac{1}{Re} \nabla^2 \omega. \tag{3.2}$$

These are written in non-dimensional form with attachment-line boundary-layer edge velocity (U_{1e}) as the velocity scale and the displacement thickness at the inflow (δ_{in}^*) (as shown in figure 2) as the length scale. All other scales are derived from these two and the Reynolds number (Re) in (3.2) is given by, $Re = U_{1e}\delta_{in}^*/\nu$, with ν as the kinematic viscosity of the medium.

The present formulation is different on a few counts from that discussed in Peridier *et al.* (1991*a,b*). First, the present problem is for a convecting vortex that induces an instability over an existing steady boundary layer. Secondly, the equations that are solved (given by (3.1) and (3.2)) are the full Navier-Stokes equation in Eulerian description using ψ and ω as dependent variable. Thus, the accuracy of the solution with respect to satisfying mass conservation is ensured.

4. Numerical methods and auxiliary conditions

The details of the numerical methods used here are to be found in Sengupta *et al.* (2004), and only a brief outline of the same is provided. Equations (3.1) and (3.2) are solved in the physical (x, y)-plane, with uniform grid in the streamwise direction and a stretched grid in the wall-normal direction.

A stabilized bi-conjugate gradient algorithm is used to solve the streamfunction equation. The vorticity transport equation is solved by representing the diffusion term by central differences and the convection terms by the high-accuracy compact difference scheme described in Haras & Ta'asan (1994) and Sengupta *et al.* (2003*a*). The scheme developed in Haras & Ta'asan (1994) was strictly for periodic problems, that was extended for non-periodic problems in Sengupta *et al.* (2003*a*) with special boundary stencils, as given in (4.1), (4.2), (4.4) and (4.5) below, so that the overall scheme is globally stable. The compact scheme used here is given by the following stencils, with subscripts indicating the node locations,

$$u_1' = \frac{1}{2h}[-3u_1 + 4u_2 - u_3], \tag{4.1}$$

Case	c/U_{1e}	h/δ^*_{in}	$\Gamma/U_{1e}\delta^*_{in}$	x_v/δ^*	r_0/δ^*_{in}	x_{in}/δ^*_{in}	x_{out}/δ^*_{in}	$Re_v = \Gamma/\nu$
1	0.2	30.0	50.0	50.0	6.0	150.0	550.0	211.063
2	0.2	30.0	−30.0	50.0	6.0	150.0	350.0	126.638

TABLE 1. Comparison of two cases.

$$u'_2 = \frac{1}{h}\left[\left(\tfrac{2}{3}\beta - \tfrac{1}{3}\right)u_1 - \left(\tfrac{8}{3}\beta + \tfrac{1}{2}\right)u_2 + (4\beta + 1)u_3 - \left(\tfrac{8}{3}\beta + \tfrac{1}{6}\right)u_4 + \tfrac{2}{3}\beta\, u_5\right], \quad (4.2)$$

$$\alpha u'_{l-1} + u'_l + \alpha u'_{l+1} = \frac{b}{4h}(u_{l+2} - u_{l-2}) + \frac{a}{2h}(u_{l+1} - u_{l+1}) \quad \text{for} \quad 3 \leqslant l \leqslant N - 2, \quad (4.3)$$

$$u'_{N-1} = \frac{1}{h}\left[-\left(\tfrac{2}{3}\beta - \tfrac{1}{3}\right)u_N + \left(\tfrac{8}{3}\beta + \tfrac{1}{2}\right)u_{N-1}\right.$$
$$\left. - (4\beta + 1)u_{N-2} + \left(\tfrac{8}{3}\beta + \tfrac{1}{6}\right)u_{N-3} - \tfrac{2}{3}\beta u_{N-4}\right], \quad (4.4)$$

$$u'_N = \frac{1}{2h}[3u_N - 4u_{N-1} + u_{N-2}], \quad (4.5)$$

where primes in these equations indicate a first derivative evaluated at the nodes. Here, $\alpha = 0.3793894912$, $a = 1.57557379$ and $b = 0.1832051925$ are used for the interior point stencil given by (4.3). For the near boundary points, $\beta = 0.06$ for $l = 2$ in (4.2) and $\beta = 0.11$ for $l = N - 1$ in (4.4) are used. The interior stencil is an optimal one for periodic problems and the spectral resolution of the interior scheme is very high in comparison to other compact schemes. To control aliasing while retaining numerical stability, an explicit fourth-order dissipation term is added at every point. This has been discussed in Sengupta *et al.* (2004).

For the convected potential vortex outside the shear layer, we can calculate the induced velocity field at the inflow and the top of computational domain analytically. The streamfunction due to a single convected irrotational vortex of strength, Γ, of core radius r_0 is given by,

$$\psi = -(U_{1e} - c)\left[\frac{(y-h)r_0^2}{\bar{x}^2 + (y-h)^2} + \frac{(y+h)r_0^2}{\bar{x}^2 + (y+h)^2}\right] + \frac{\Gamma}{4\pi}\ln\frac{\bar{x}^2 + (y+h)^2}{\bar{x}^2 + (y-h)^2}, \quad (4.6)$$

where $\bar{x} = x - ct$, with c as the convection speed of the vortex. The height of the vortex over the boundary is given by h. This expression is used to calculate the time-dependent boundary conditions for solving (3.1) and (3.2).

Navier–Stokes equations have been solved using a (501×101) grid with 501 points in the streamwise direction distributed uniformly for case 1, given in table 1. In the wall-normal direction, the grid points are non-uniformly distributed up to $y_{max} = 16\delta^*_{in}$ with the wall resolution given by $1.8 \times 10^{-3}\delta^*_{in}$. The points are distributed in an arithmetic progression in this direction, as it is known (Sengupta 2004) to produce grid-independent accurate results. The rationale for the choice of grid and numerical methods is discussed in Sengupta *et al.* (2004). The outflow boundary condition used here is given by $\partial\omega/\partial t = 0$, which allows the disturbance to pass the domain without any reflections.

5. Results and discussion

The unperturbed flow field is obtained using a uniform grid with 1800 points, so that the mean flow is calculated with adequate accuracy, up to a maximum non-dimensional similarity coordinate $\eta_{max} = 16$. This solution is interpolated using cubic splines at the 101 nodes used for solving (3.1) and (3.2). As the physical coordinate and the similarity variable are related by, $\eta = \sqrt{((m+1)U_{1e}/2\nu x^*)}\, y^*$, the boundary-layer displacement thickness is obtained from $\delta^*(x) = \int_0^\infty (1-g)\,\mathrm{d}y^* = \sqrt{(\nu x^*/U_{1e})} \int_0^\infty (1-g)\,\mathrm{d}\eta$.

For the attachment-line boundary layer, the quantity $\delta = \int_0^\infty (1-g)\,\mathrm{d}\eta$ is obtained from the similarity solution as 1.027286. As the displacement thickness (δ_{in}^*) at the inflow is taken as the length scale for non-dimensionalization, then $y = y^*/\delta_{in}^* = \eta(x_{in}^*)/\delta$ and $x = x/\delta_{in}^* = \sqrt{(U_{1e}/\nu x_{in}^*)}\, x^*/\delta$. Thus, the displacement thickness at the inflow is obtained as $\delta_{in}^* = \delta^2 x_{in} \nu/U_e$; and the corresponding Reynolds number is given by $Re_{\delta^*} = U_{1e}\delta_{in}^*/\nu = \delta^2 x_{in}$.

For the chosen similarity profile, δ is fixed. Hence, by fixing x_{in} we fix the Reynolds number at the inflow. This is the Reynolds number that appears in (3.2). In the present exercise, two sub-critical excitation cases have been considered whose parameters are given in table 1. In Lim *et al.* (2004) it was seen that for a Blasius boundary layer the counterclockwise rotating (positive) vortex caused bypass transition ahead of the vortex, while the clockwise rotating (negative) vortex creates a moving bubble(s) behind the vortex at the onset. The two cases table 1 are chosen to investigate whether similar differences exist when the attachment-line shear layer is excited by vortices of opposite signs.

In table 1, the second column indicates the speed of convection of the vortex, as shown in figure 2. The third column provides the non-dimensional height of the vortex from the leading edge of the wing. The non-dimensional strength of the vortex is given in the fourth column. x_v is the initial streamwise location of the vortex and r_0 is the core size of convecting vortex. The inflow and outflow of the computational domain are indicated by x_{in} and x_{out}, respectively. In the last column, the strength of the vortex is defined via a Reynolds number given by, $Re_v = \Gamma/\nu$. In Sengupta *et al.* (2004), numerical results were reported for a very wide range of Re_v investigating various sub- and super-critical excitation cases. For the two cases discussed here, the speed of convection, the core size, height and initial location of the vortex are kept identical. The sign of the vortex is opposite in case 2 and with a lower vortex strength.

5.1. *Bypass transition*

The first case considered here corresponds to a single potential vortex of counter-clockwise circulation convecting at a speed of $0.20U_\infty$ over the leading edge of the infinite swept wing at a height of $30\delta_{in}^*$. This case is investigated here in detail, because it was shown in SDS that a counterclockwise vortex creates bypass transition very effectively for a Blasius boundary layer. This was also seen for the numerical simulation cases in Sengupta *et al.* (2004) for the LEC problem for different parameter combinations. In comparison to those cases, here the convecting vortex is made to move at a higher height, thereby showing the stronger receptivity of the proposed mechanism.

In figure 3, the streamline and vorticity contours have been plotted at the indicated time instants for case 1 of table 1. For this case, the flow becomes unstable with the appearance of a bubble on the wall that starts a sequence of bubbles forming ahead of it, as seen experimentally in SDS. Frames in figure 3 are for those times when the
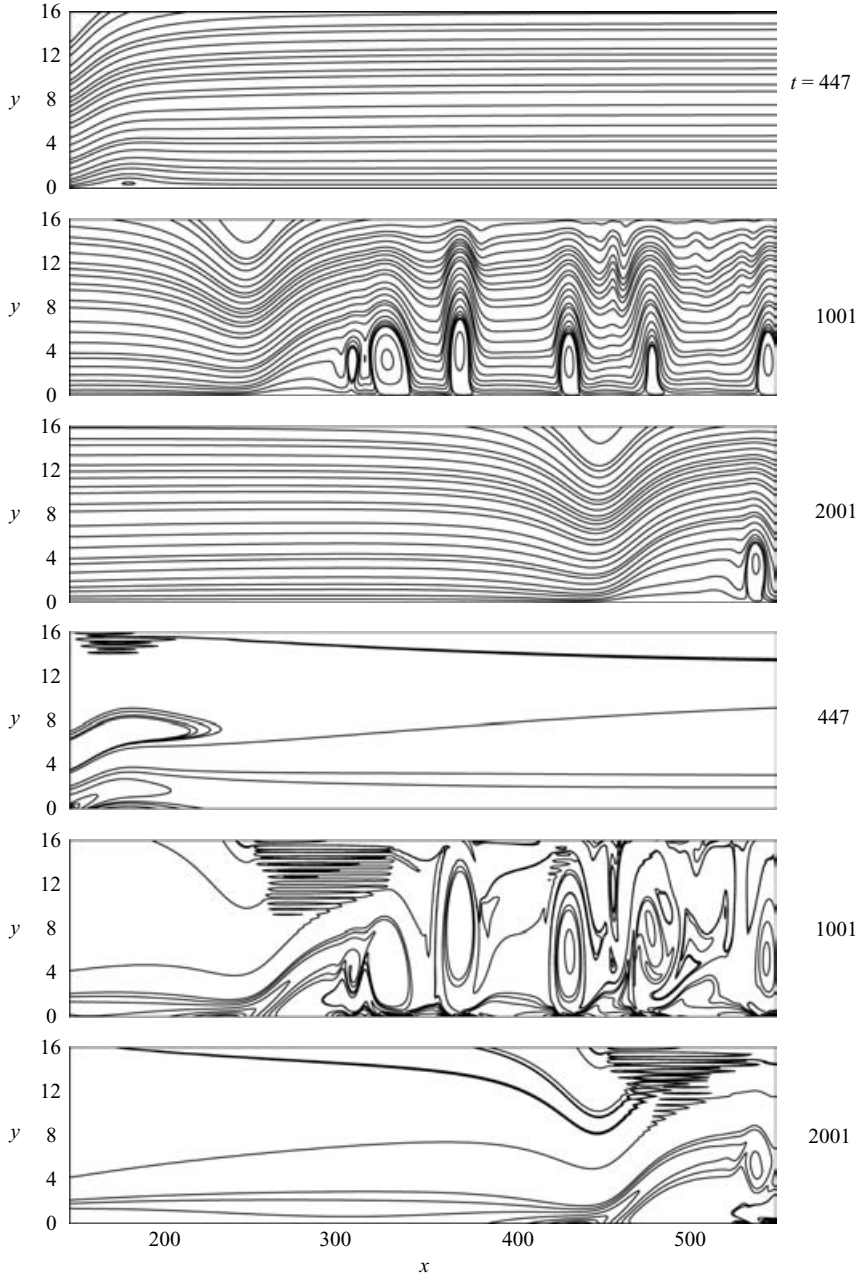
FIGURE 3. Streamline (top three panels) and vorticity (bottom three panels) contours at the indicated times for case 1.

convective vortex streamwise location are $x = 140, 250$ and 450. The feature of the excited field is that the induced instability is always ahead of the vortex. In the last frame of figure 3 the induced disturbances are seen to leave the computational domain even when the streamwise location of the vortex is within the computation domain. It is noted that the first bubble makes its appearance at $t = 417$ at a streamwise location $x = 180$ where the local Reynolds number based on displacement thickness

is $Re_{\delta^*} = 190$. The first appearance of a bubble can be considered as an indicator of flow criticality with respect to imposed external disturbance.

As the phenomenon is nonlinear, it is not possible to ascribe any fixed critical Reynolds number. For the same reason, it is not apparent how we define a transitional Reynolds number. The critical value of the Reynolds number given in Poll (1979) refers to the threshold limit of the transitional Reynolds number for the attachment-line of the tested model with respect to the disturbance environment of the tunnel. Once the first bubble forms on the wall, a succession of others follow governed by the mechanism discussed in SDS. In Obabko & Cassel (2002), the first bubble was introduced as an artefact of the model where a Batchelor vortex translating at a predefined constant speed was introduced. In contrast, in SDS, the first bubble came out as a solution of the governing equations created by the convecting vortex in the free stream. Peridier *et al.* (1991*a*) studied the stability of the unsteady shear layer that forms on the plane wall in the absence of mean convection. Noted eruptions were vertical with respect to the unsteady boundary layer. The presence of steady convection causes the eruptions to be inclined and they are also milder in SDS.

The case simulated in SDS can be viewed to model the unit process for the effect of free-stream turbulence (FST). The fact that a distant vortex can induce a small longitudinal adverse pressure gradient to destabilize a wall-bounded flow was postulated first by Taylor (1936) and is discussed in SDS. In Lim *et al* (2004), a series of experiments is reported to explain how the adverse pressure gradient is created ahead (behind) of a positive (negative) vortex migrating in the free stream. Once a single moving bubble is created, it leads to secondary instabilities whereby multiple bubbles are formed. Appearance and convection of multiple coherent bubbles make the behaviour of physical variables very intermittent. As attachment-line shear layer is more stable with respect to linear mechanism, it is of greater interest to investigate the sub-critical instability and bypass mechanism. The plotted vorticity contours help us to understand the coupling between the free-stream disturbance source and its effect within the shear layer. For example, at $t = 447$, we notice weak vortical structures simultaneously appearing inside and outside the shear layer. The mechanism of such coupling between the free-stream source and disturbances within a shear layer is explained in Sengupta *et al.* (2002), where a distinction is made between the case where the free-stream disturbance source moves with the free stream and the case where it moves at a speed lower than this. It is seen that the receptivity is higher when free-stream disturbances move at slower speeds. For this reason, the present computations show strong bypass transition as compared to that shown in Obrist & Schmid (2003*b*), where the computations displayed lower (exponential) growth rates for the introduced bubble moving at free-stream speed.

5.2. *The physical mechanism of instability*

As stated in SDS, the key to understanding bypass transition is to trace the evolution of total mechanical energy associated with the flow during the instability – a proper measure of it for incompressible flow is $E = p/\rho + V^2$. This is split into a mean and a disturbance component. In SDS, the equation for disturbance energy (E_d) was shown to be governed by the Poisson equation,

$$\nabla^2 E_d = 2\boldsymbol{\omega}_m \boldsymbol{\omega}_d + \boldsymbol{\omega}_d \cdot \boldsymbol{\omega}_d - V_m \cdot \nabla \times \boldsymbol{\omega}_d - V_d \cdot \nabla \times \boldsymbol{\omega}_m - V_d \cdot \nabla \times \boldsymbol{\omega}_d. \qquad (5.1)$$

In this equation, V and ω represent velocity and vorticity fields, respectively. The subscripts m and d refer to mean and disturbance quantities. The mean field is that given by the solution of the Falkner–Cooke–Skan velocity profile defined in §2. From

the instantaneous velocity and vorticity field, we can calculate the disturbance velocity and vorticity components. Hence, the forcing terms of (5.1) is obtained at any instant. It is, therefore, possible to solve the above Poisson equation to find the distribution of the disturbance energy at any time. However, it is not necessary to solve (5.1) for finding the disturbance energy distribution in the flow field, as was shown in SDS where the property of the Poisson equation was exploited to do so. As (5.1) governs the disturbance energy, so the non-zero right-hand side indicates either source or sink of disturbance energy depending on its sign. If we accept the datum of disturbance energy as the condition prevailing in the absence of disturbances, then the growth of disturbance would be signalled by the appearance of a negative quantity on the right-hand side of (5.1).

From (5.1), we can separate out the linear and nonlinear contributions arising out of how the velocity and vorticity field interact with each other and also with itself. For example, the second and the last terms on the-right-hand side of (5.1) represent nonlinear contributions to the disturbance energy. The self-induced effect of vorticity field, as represented by the second term, always contributes locally in creating an energy sink, whereever it is significant. We cannot make any general observation on the other nonlinear term.

To have a better understanding of the flow instability for the present case, in figure 4(*a, b*), different contributions arising out of different sets of terms have been plotted in the top three frames. On the top frame, the nonlinear vorticity inter-action dominates over the nonlinear contribution arising from the interaction between the velocity and vorticity fields at early times. Thus, the primary instability is due to vorticity–vorticity interaction. Later on, secondary instabilities due to velocity–vorticity interaction becoming dominant, as shown in figures 4(*a*) and 4(*b*). In these figures, the third frame indicates the total right-hand side of (5.1) in which the white patches indicate the flow region where the right-hand side represents disturbance energy sinks. Comparing these figures with vorticity contours in figure 3, we notice that the negative contours arising out of vorticity–vorticity interaction correlate best with the forming vortical structures at the wall. The secondary structures seen off the wall are essentially due to the vorticity–velocity interaction terms. Similar correlation was seen in SDS for the Blasius profile, implying a generic nature for these interactions. As the instability grows into bypass transition, the disturbance energy sources and sinks alternately become sites for vortices of opposite signs and their interactions give rise to the observed eruptions. The creation of coherent structures of opposite signs starts secondary flow from sources to sinks that are responsible for significant unsteadiness.

It is noted that the disturbance energy equation arises by taking the divergence of the Navier–Stokes equation in the rotational form, representing the irrotational compon-ent of the disturbance field. The rotational field of the Navier-Stokes equation as given by the vorticity transport equation yields the Orr–Sommerfeld equation obtained by linearization and making the parallel-flow approximation. Although Morkovin (1991) suggested that unsteadiness during bypass transition is due to the shear noise term in the Poisson equation for the static pressure, to our knowledge, no previous efforts have interpreted instabilities in terms of this disturbance energy equation.

These events being highly unsteady, it is of interest to estimate the time rate of these instabilities. The calculated time-rate contours of the source–sink terms of (5.1) are obtained numerically and plotted in the lowermost panels of figure 4(*a, b*). In all frames of figure 4, maximum and minimum values of various quantities plotted are indicated. A negative time rate would indicate that the source strengths are increasing, if it is in the negative contour region.
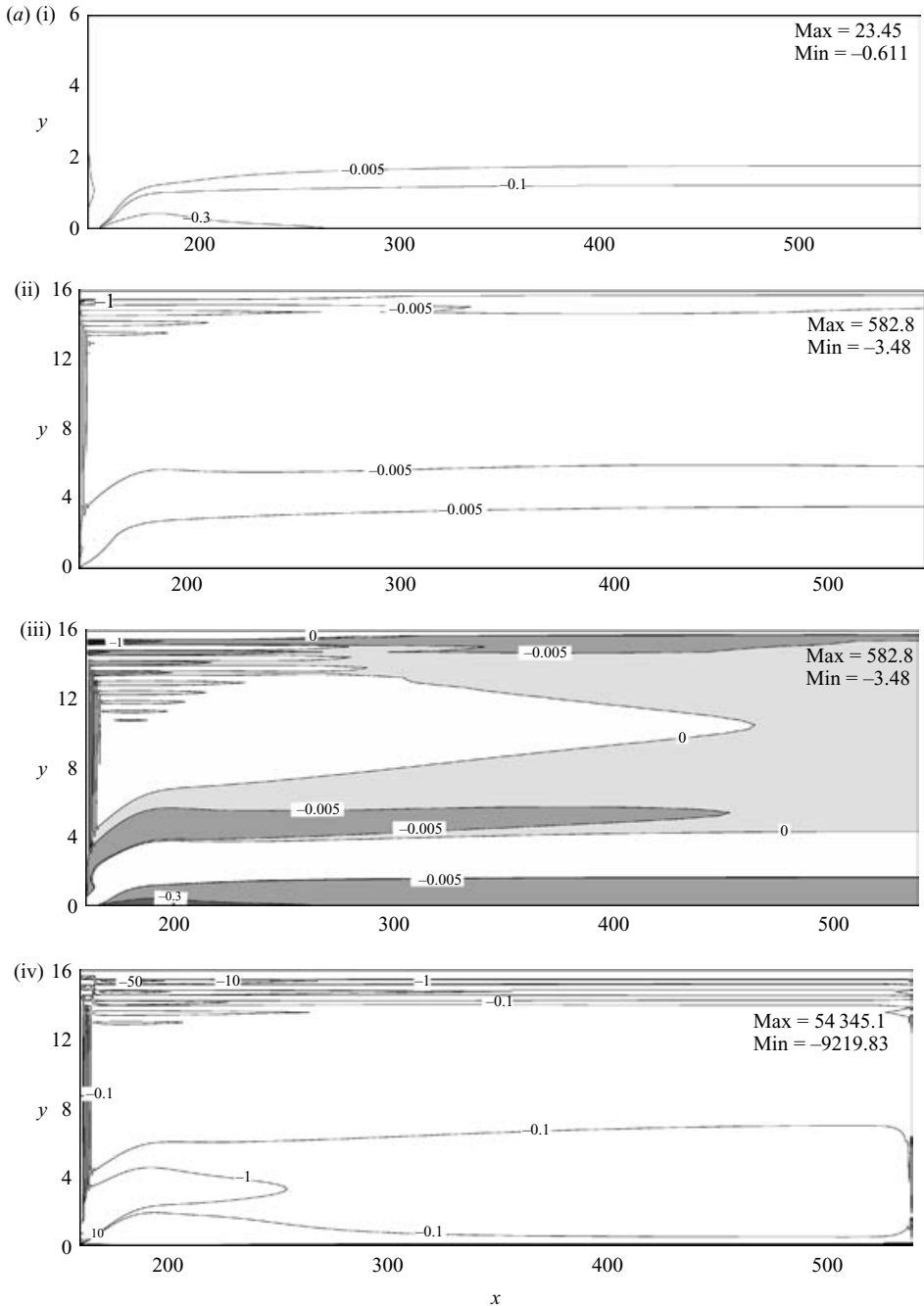
FIGURE 4. For legend see facing page.

The actual flow over a finite sweptback wing is more complicated owing to the presence of many vortices as trigger. To understand the unit process, a single vortex is convected at a constant height, as was also done in the experiments in Lim *et al.* (2004) and Sengupta *et al.* (2001). Presence of multiple vortices lead to complex Biot-Savart interactions that would cause the vortices to move with non-uniform speed.
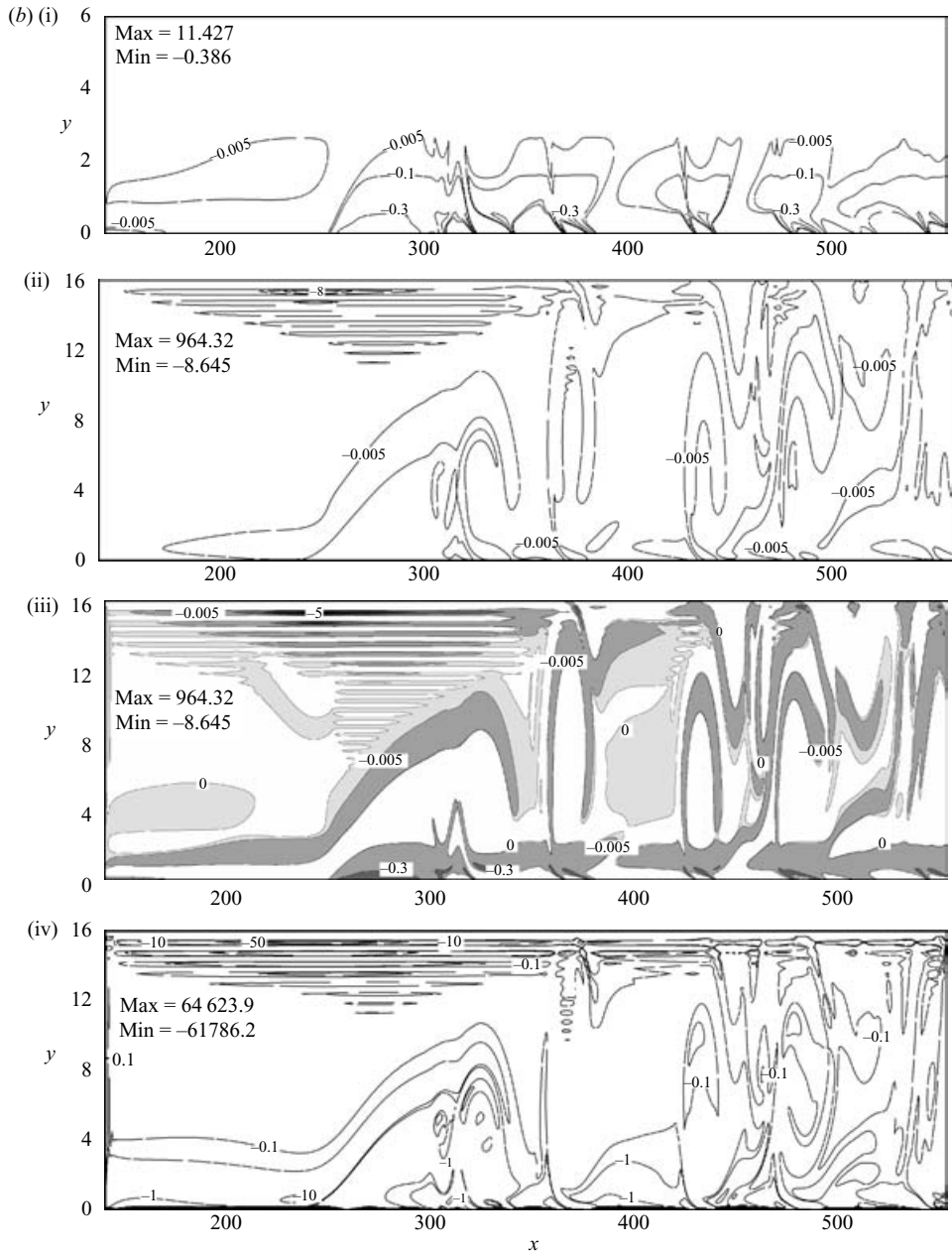
FIGURE 4. Contour plots of the disturbance energy source terms, (i)–(iii), and its time rate indicating the regions where the instability increases, (iv). (*a*) $t = 447$, (*b*) 1001. (i) Vorticity–vorticity; (ii) velocity–vorticity; (iii) complete (nonlinear); (iv) time rate of source term.

This will bring in additional issues of acceleration (or deceleration) effects, resulting in vortices moving in complex trajectories.

The equation of receptivity (5.1), is based on full Navier-Stokes equation without any simplifying assumptions. Hence, it is the most generic equation for flow instability. Also, it is valid for both two- and three-dimensional incompressible flows. Thus,

significant unsteadiness with large spectral bandwidth disturbances can be created without a vortex stretching mechanism to explain small-scale features of transitional and turbulent flows. Once the attachment-line flow becomes unstable by the vortex-induced instability, its effect will be felt off the attachment-line, an issue addressed in Theofilis *et al.* (2003) and Obrist & Schmid (2003*a*) under linear instability framework.

In Sengupta *et al.* (2004) the receptivity of LEC to different parameters is reported, leaving out the negative vortex case. The case 2 of table 1 is one such case where a negative vortex of lower strength (as compared to case 1) migrates over the attachment-line and is studied next.

5.3. *Effects of a convecting negative vortex*

All the parameters for this case is given in table 1. It was noted experimentally in Lim *et al.* (2004) that a negative vortex creates an adverse pressure gradient behind it and hence instability begins upstream of the vortex. The streamline and vorticity contours for this case are shown in figure 5. Instantaneous streamwise location of the free-stream vortex is identified by an arrowhead in streamline contour plots. The first bubble forms upstream of the convecting vortex, as seen for $t = 804$. However, beyond $t = 1005$ the bubble created by the primary instability of the underlying shear layer overtakes the convecting vortex. As explained in the previous section and in Sengupta *et al.* (2001), there prevails a favourable pressure gradient ahead of the vortex for a vortex of negative sign. Thus, once the bubble overtakes the free-stream vortex, its strength and vertical size decreases. The stabilizing effect of the favourable pressure gradient can also be seen from the vorticity contours of figure 5. Whether the created bubbles would overtake the free-stream vortex or not depends on the parameter combinations of table 1. For example, in Lim *et al.* (2004) created bubbles for the Blasius layer always trailed behind the clockwise rotating free-stream vortex with attendant secondary instabilities. The present case is characterized by the absence of secondary instability.

The corresponding right-hand side of (5.1) plotted for case 2 is shown in figure 6. Once again, at early times the primary instability arises due to vorticity–vorticity interaction. In figure 6(*a*), it is seen that the velocity–vorticity interaction gives rise to a weaker source above the shear layer, apart from the strong source at the wall. This was seen in the vorticity contour plots of figure 5. However, as the local flow speed is significantly high at this height, closed contours are not seen in streamline plots. This weak vorticity source is also seen at $t = 1005$ in figure 6(*b*), with the structure elongated in the streamwise direction. With time, this weak vortical structure elongates further in both the up- and down-stream direction. However, the source strength at the wall progressively decreases, thereby weakening the bubble.

6. Characterizing LEC By POD

Coherent structures created during bypass transition can be viewed as the eigen-mode of the vorticity field obtained by POD analysis following the method of snapshot due to Sirovich (1987) and Rajaee *et al.* (1994).

This method is efficient as the number of snapshots (M) used is significantly lower than the number of grid points (N) in the domain. For the present purpose, we have used twenty snapshots ($M = 20$) centred around different times, as indicated in table 2 for time intervals of 20, while performing POD in a spatial domain with (501×101) points using the fluctuating vorticity data. The mean is calculated by an average over the chosen twenty frames and the fluctuations calculated by subtracting this from the
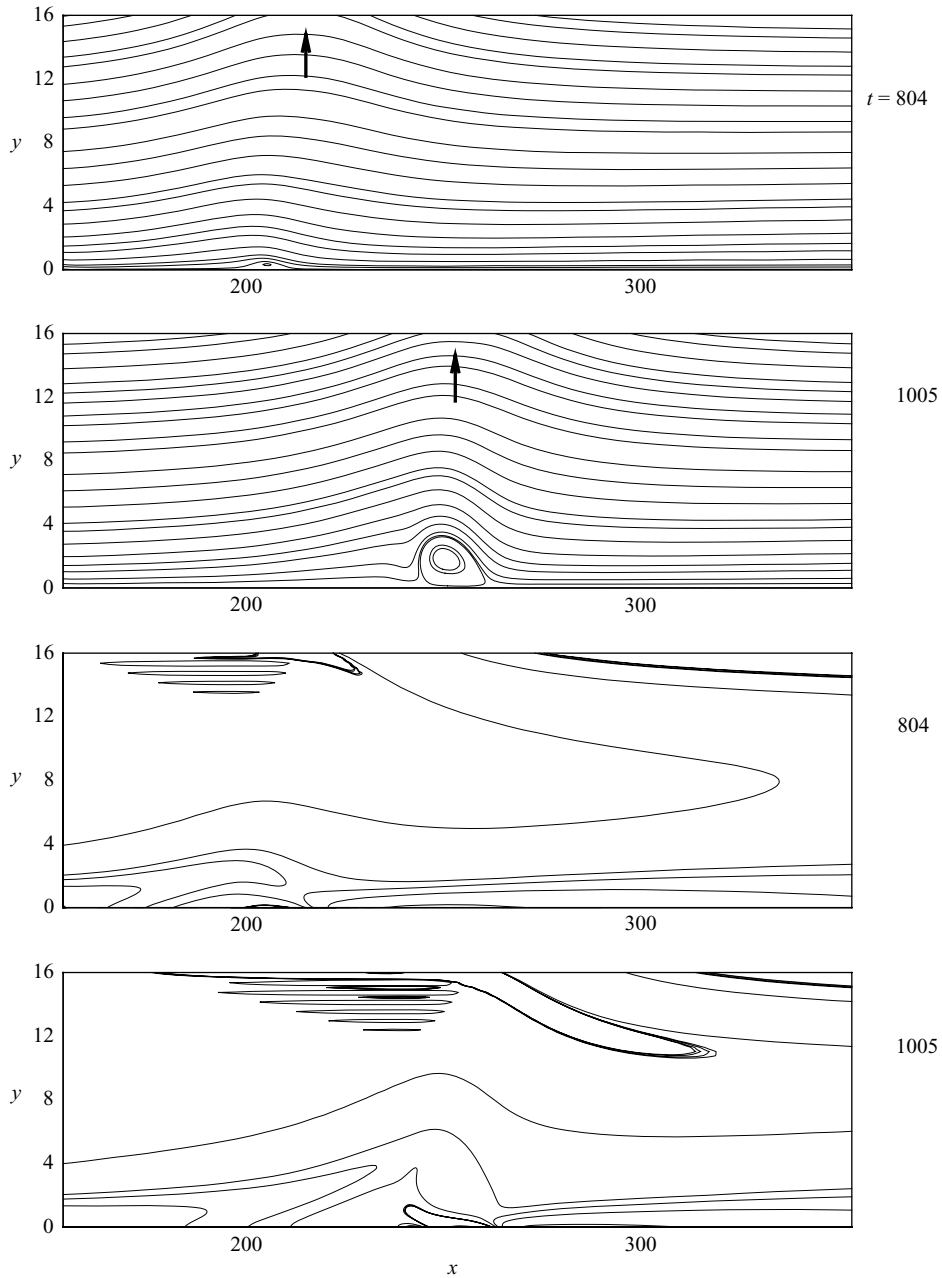
FIGURE 5. Streamline (top two panels) and vorticity (bottom two panels) contours at the indicated times for case 2.

instantaneous realizations. In table 2, the eigenvalues have been catalogued for cases 1 and 2, respectively. It is seen that the first five modes carry more than 97.5 % of the enstrophy for both the cases. The requisite number of modes carrying the same quantum of enstrophy increases for case 1, after the bypass transition begins.

In the top panel of figure 7 enstrophy content – the summation of eigenvalues – versus the number of eigenmodes in the summation is plotted for case 1. The dotted

FIGURE 6. For legend see facing page.

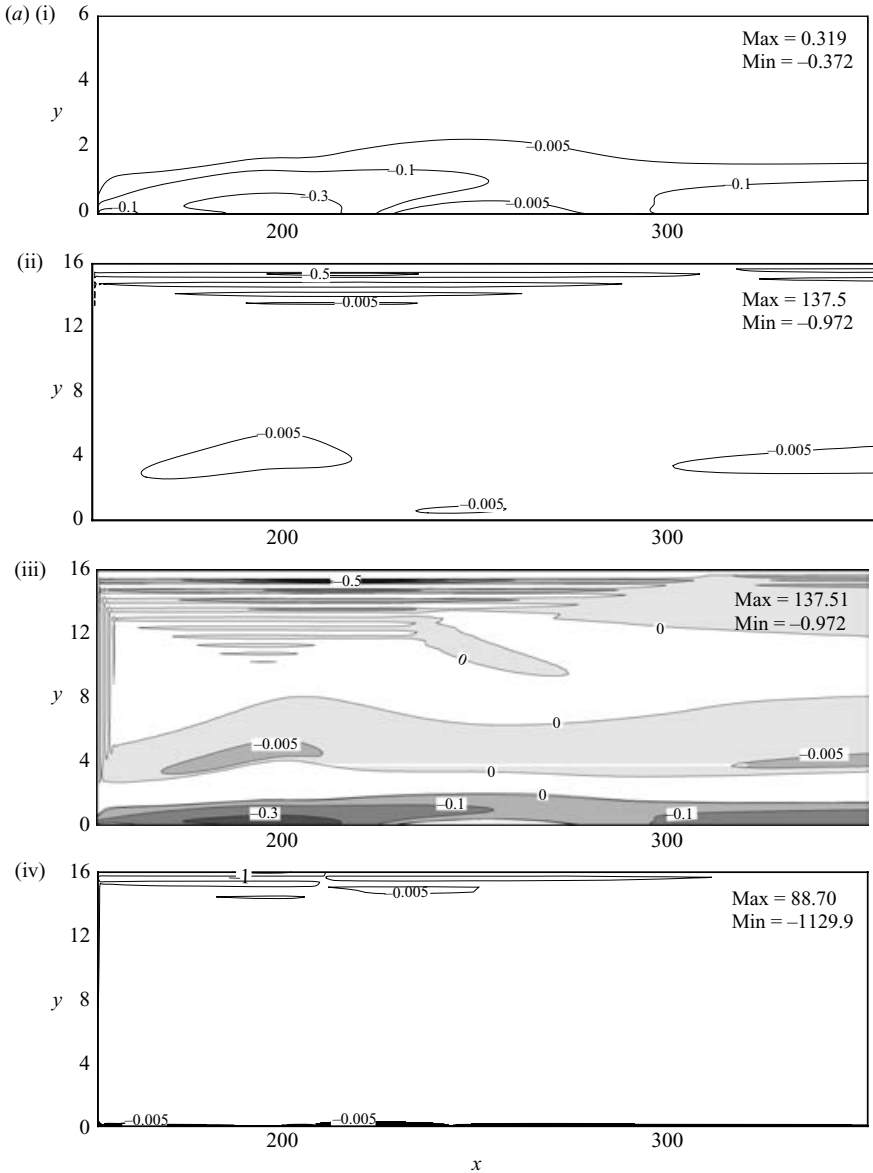line marks 99 % of the enstrophy level and it is clear that the first seven modes account for it after the onset of bypass transition during $t = 443$ to 462. The first three modes account for more than 92.5 % at all times. In figures 7(*b*) and 7(*d*) the first and second eigenmodes are shown, respectively, for the time interval during $t = 443$ to 462. In figures 7(*c*) and 7(*e*), these are shown for the time interval $t = 1007$ to 1026. These modes account for most of the vorticity production and trace the evolving coherent structures, including the view that the process originated by excitation from the free stream, as shown by the presence of fingers that connect the free-stream mode with the wall mode. Similar structures were also shown in Obabko & Cassel (2002) and its
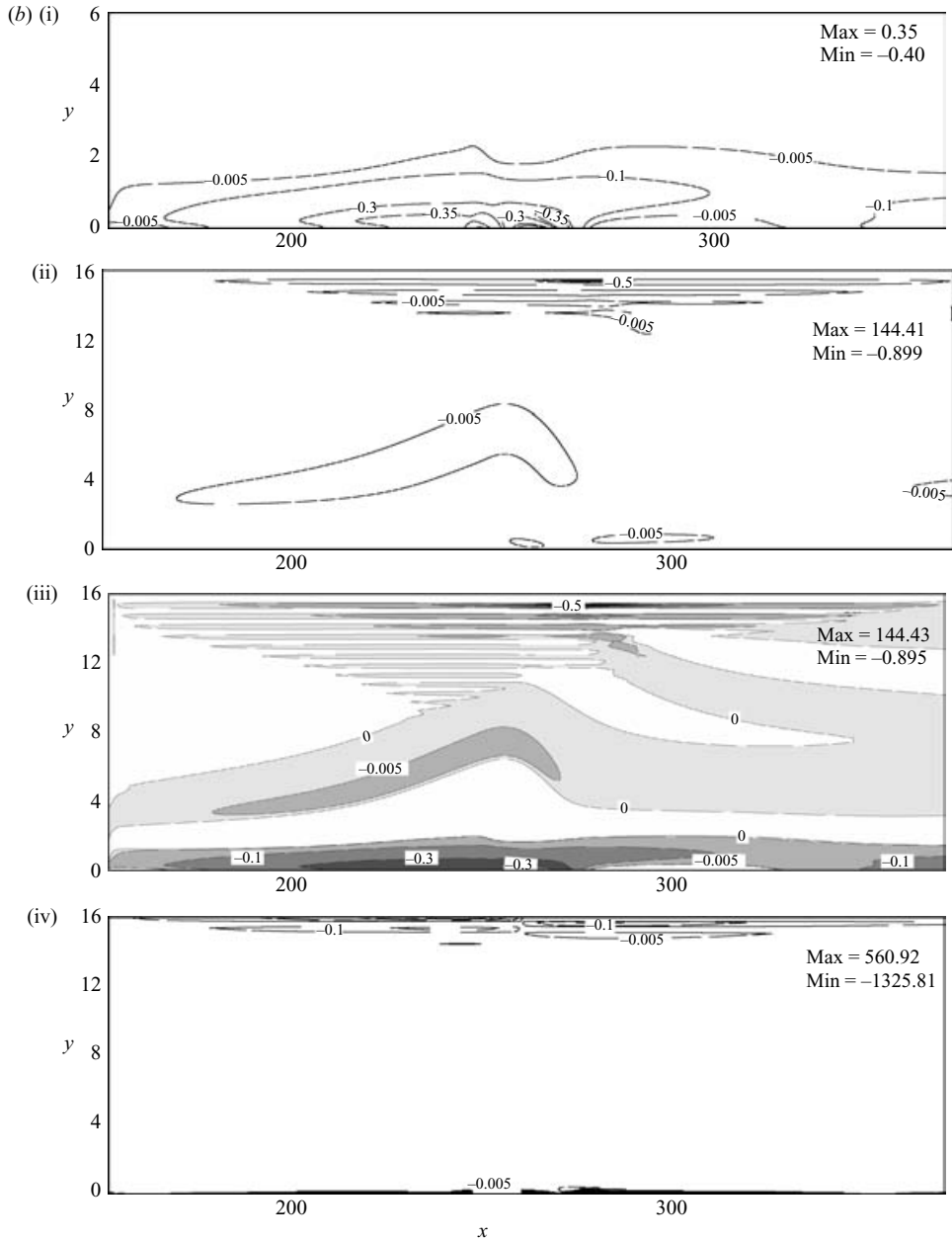
FIGURE 6. Contour plots of the disturbance energy source terms (i)–(iii), and its time rate indicating the regions where the instability increases, (iv). (*a*) $t = 804$, (*b*) 1005. (i) Vorticity–vorticity; (ii) velocity–vorticity; (iii) complete (nonlinear); (iv) time rate of source term.

theoretical explanation provided in Sengupta *et al.* (2002). All lower modes display similar spatial structures and their relative importance can be found from figure 7(*a*). The detailed information of the first ten modes is given in table 2(*a*) for providing a quantitative measure for the noted bypass transition.

(*a*)

Serial mode	Time interval, t				
	443–462	748–767	1007–1026	1501–1520	2000–2019
1	0.0621	38.7785	41.7824	19.1695	2.6302
2	0.0031	13.2259	16.4932	4.0555	0.4790
3	0.0008	3.9393	5.1122	1.2493	0.0372
4	0.0004	2.0568	2.2227	0.6120	0.0097
5	0.0003	1.0120	1.0657	0.2982	0.0038
6	0.0002	0.5872	0.5652	0.1663	0.0013
7	0.0001	0.3303	0.3021	0.0841	0.0004
8	8.37×10^{-5}	0.1981	0.1723	0.0439	0.0002
9	5.13×10^{-5}	0.1179	0.0921	0.0214	5.65×10^{-5}
10	2.73×10^{-5}	0.0699	0.0532	0.0109	2.25×10^{-5}

(*b*)

Mode number	Time interval, t				
	501–520	805–824	1005–1024	1200–1219	1407–1426
1	0.0046	0.0252	0.2122	0.1631	0.0353
2	0.0028	0.0004	0.0062	0.0098	0.0052
3	2.21×10^{-5}	1×10^{-4}	0.0025	0.0051	0.0006
4	3.60×10^{-6}	4.97×10^{-5}	0.0002	0.0005	0.0003
5	2.04×10^{-6}	4.44×10^{-6}	0.0002	0.0002	5.22×10^{-5}
6	1.66×10^{-7}	1.77×10^{-6}	0.0001	0.0001	5.86×10^{-6}
7	2.90×10^{-8}	7.57×10^{-7}	3.13×10^{-5}	4.16×10^{-5}	2.60×10^{-6}
8	8.09×10^{-9}	1.72×10^{-7}	1.05×10^{-5}	2.09×10^{-5}	4.43×10^{-7}
9	1.98×10^{-9}	5.55×10^{-8}	2.26×10^{-6}	1.06×10^{-5}	2.34×10^{-7}
10	7.07×10^{-10}	1.27×10^{-8}	8.06×10^{-7}	6.24×10^{-6}	4.14×10^{-8}

TABLE 2. Eigenvalues for cases 1 and 2.

For case 2, the excitation causes vortical structure to appear behind the vortex owing to a primary instability. The excited disturbances are far weaker than that for Case 1 and no secondary instabilities are seen. Corresponding cumulative enstrophy content at different time intervals is shown in figure 8(*a*). In this case, only the first mode dominates and it is shown in figures 8(*b*) and 8(*c*) for the indicated time intervals. These snapshots show the evolution of vortical structures inside the shear layer. Once again, we can relate this structure with convecting free-stream vortex via the appearance of fingers. For quantitative comparison, the first ten eigenvalues are given in table 2(*b*) for the indicated time intervals.

7. Pattern formation during instabilities

From the results of the previous sections, it is noted that the bypass transition occurring during LEC is characterized by evolution of coherent vortical structures that are shown in vorticity contour plots in figure 3 for case 1 and in figure 5 for case 2. These structures were also seen in POD eigenmode plots of figures 7 and 8 for the two cases described in this paper. The tendency to form coherent structures can be detected even earlier, if one were to plot the time rate of the right-hand side of (5.1) much before the onset of instability as shown in vorticity contour plots.
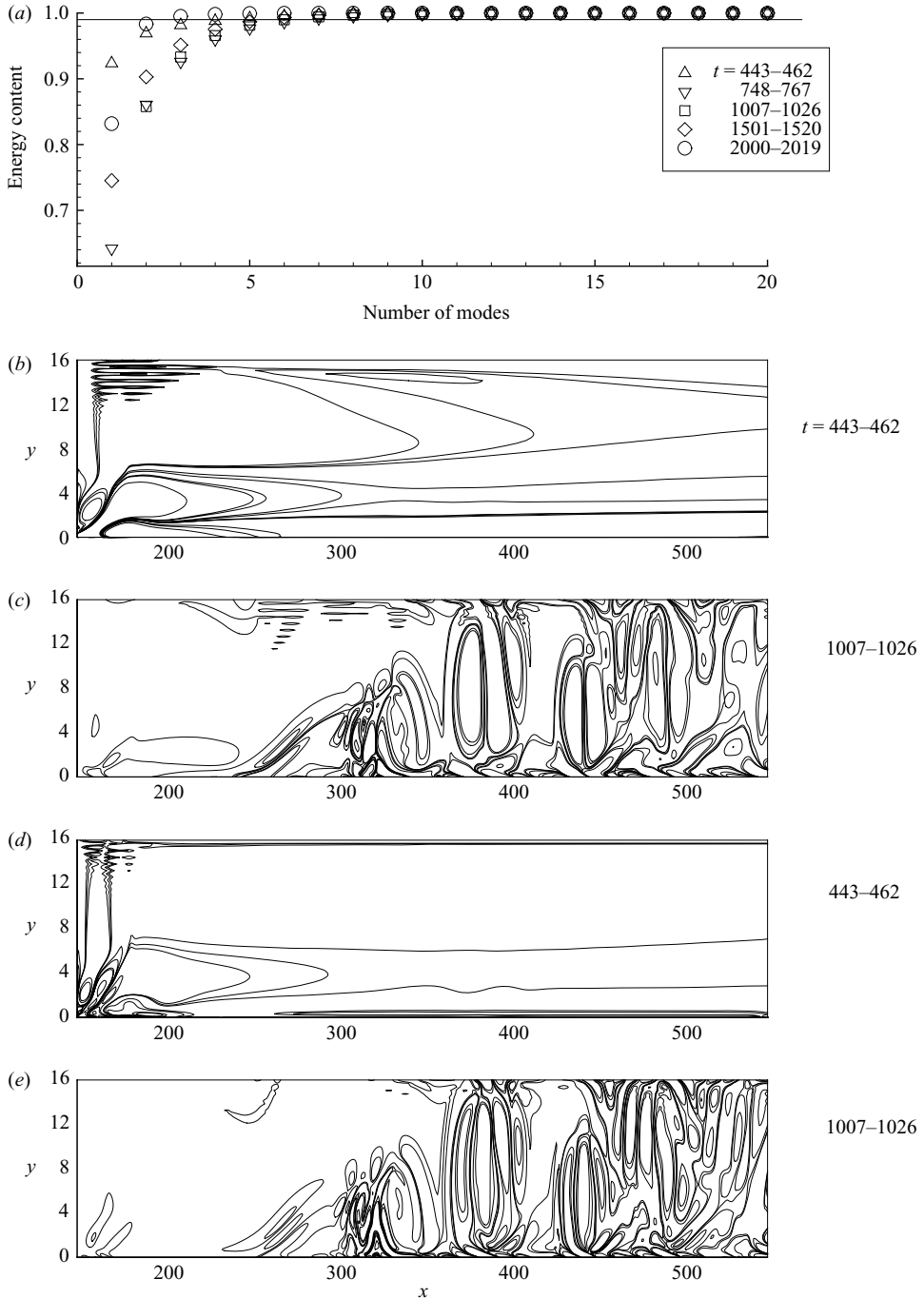
FIGURE 7. (*a*) The eigenvalues and (*b*–*e*) the eigenfunctions of disturbance vorticity for case 1. (*a*) The energy content, sum of eigenvalues *vs.* the number of modes; (*b*), (*c*) are for the first eigenmode and (*d*), (*e*) for the second.

For both cases, such time rates are shown in the bottom panels of figures 4(*a*), 4(*b*), 6(*a*) and 6(*b*) at the indicated times. In figure 9(*a*) the contours of time rate of formation of energy sources (negative contour values) and sinks (positive contour
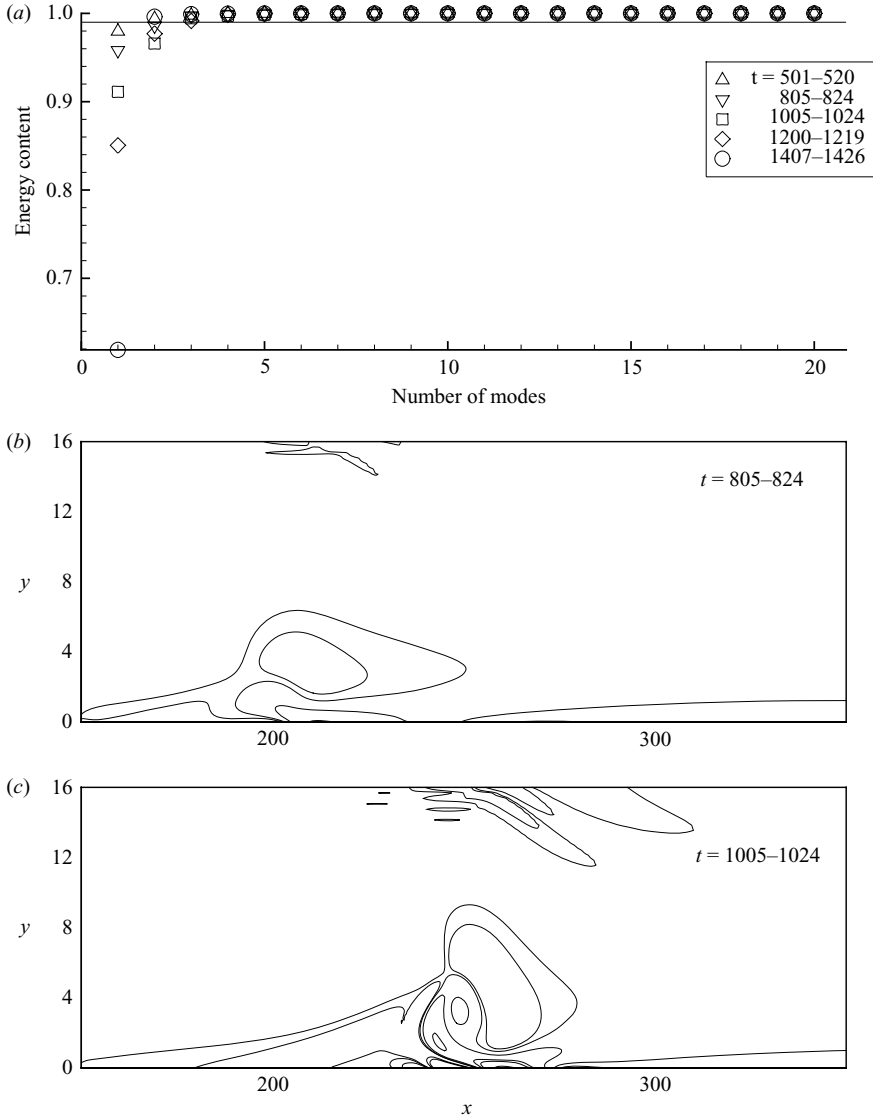
FIGURE 8. (*a*) The eigenvalues and (*b, c*) the eigenfunctions of disturbance vorticity for case 2. (*a*) The energy content, sum of eigenvalues, *vs.* the number of modes; (*b*), (*c*) are for the first eigenmode.

values) are shown. The primary instability structure is identified as *A* in the panels and is seen at $t = 402$. These appear as regular elongated geometrical cellular structures. For case 1, this appears as a spike growing vertically at the primary instability site of alternate signs. Similar cellular structures were also seen for the Blasius boundary layer and hence these structures are generic for external flows.

In figure 9(*b*), formation of such cellular structures are shown for case 2 at the indicated time frames. In this case, the evolving structures are flatter as compared to case 1. Very weak secondary structures appear following the primary instability and are seen at $t = 1005$.
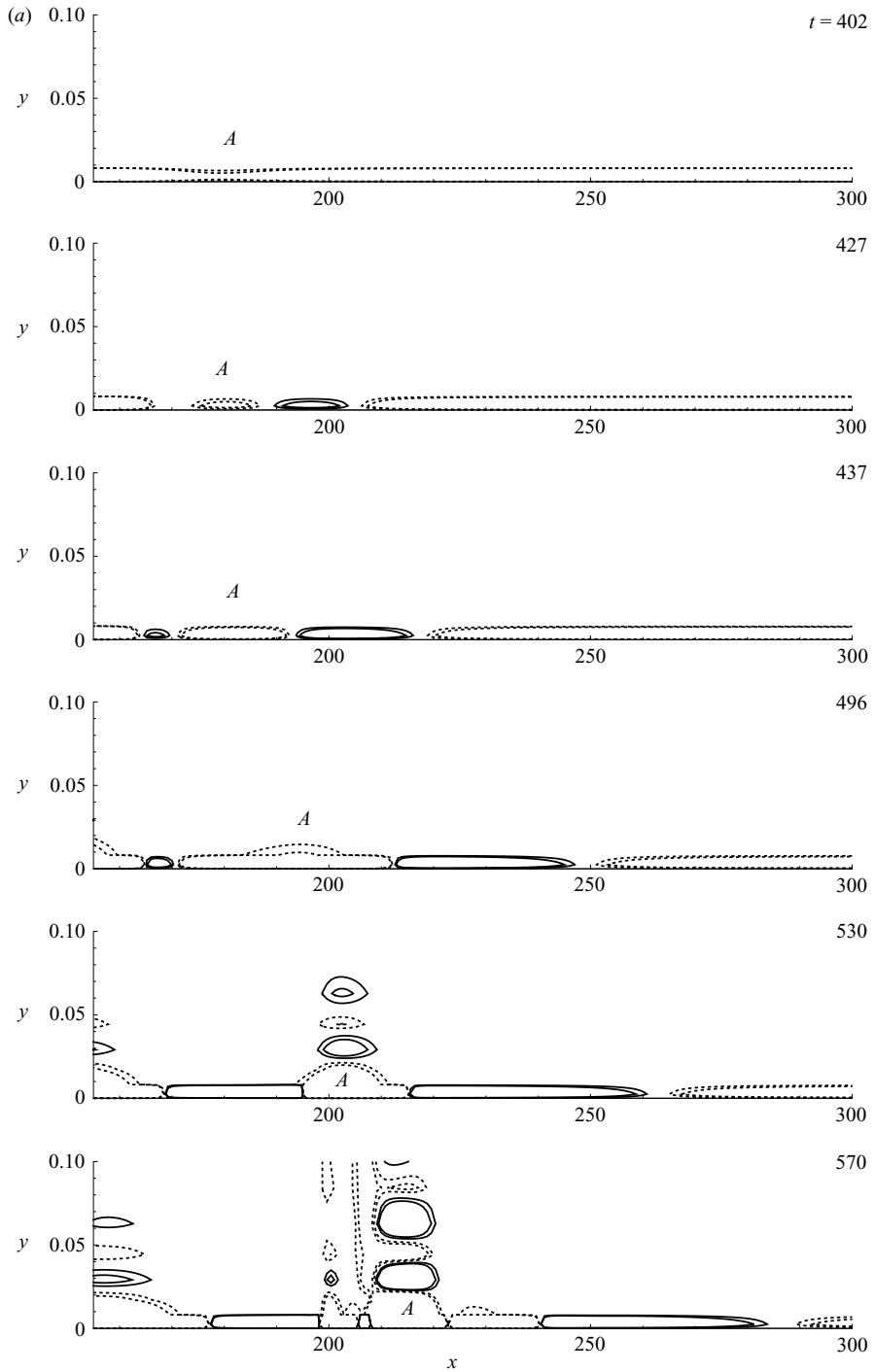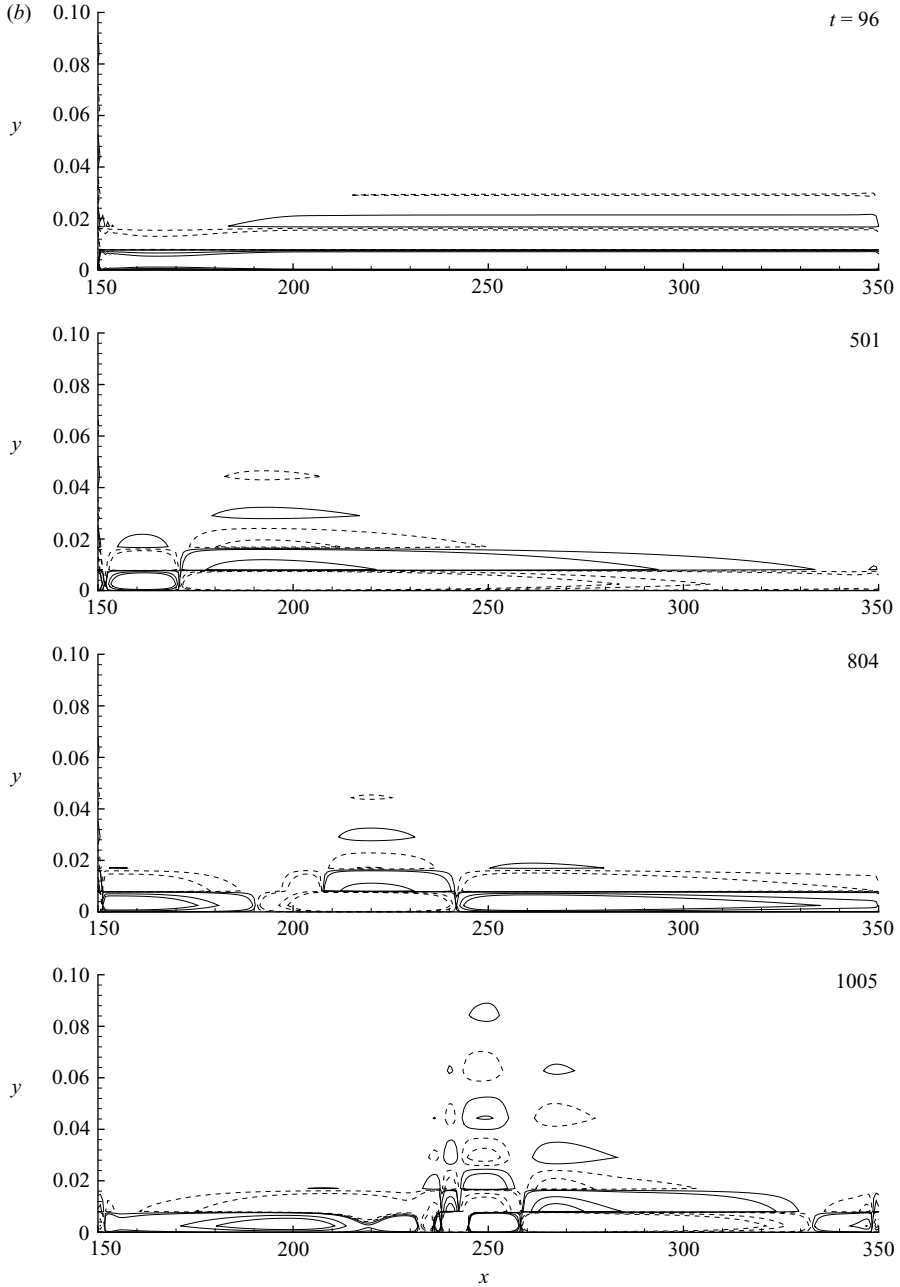
FIGURE 9. For legend see next page.

FIGURE 9. Near-wall cellular structure at indicated times, (*a*) for case 1, (*b*) for case 2. Negative contours are shown by dashed lines.

8. Concluding remarks

Here, we present a new interpretation for leading edge contamination of an infinite swept wing as being caused by convecting vortices in the free stream. This is shown as subcritical instability of the swept Hiemenz flow in the attachment-line plane via the solution of the two-dimensional Navier–Stokes equation by high-accuracy compact

schemes. This bypass transition is similar to that shown in SDS for the zero-pressure-gradient boundary layer. The main aim here is to provide the physical mechanism behind the observed spatio-temporal instability and this is made possible with the help of the receptivity equation (5.1), that was introduced in SDS. It is established as vortex-induced instability which is caused by a small local adverse pressure gradient over the shear layer. The resultant unsteady separated flow suffers a further sequence of secondary instabilities for the case of positive convecting vortex outside the shear layer. This type of scenario was experimentally demonstrated in Sengupta *et al.* (2001) and Lim *et al.* (2004) for subcritical instability of the Blasius boundary layer. Apart from showing the physical mechanism, we also provide the time-growth rate of the noted instability. It is also established that only a positive (counterclockwise) vortex causes the bypass transition ahead of the convecting vortex. As observed for the Blasius boundary layer, the negative (clockwise) vortex has very weak receptivity for the attachment-line shear layer.

Furthermore, using the numerical simulation data, we perform POD analysis following the method of snapshots due to Sirovich (1987). This analysis clearly shows that only a few modes are responsible for the observed instability. The enstrophy associated with the instability is presented along with the associated eigenmodes. The presented results in this paper provide a new mechanism for LEC that can be termed the bypass transition. This is already shown as a subcritical instability via the experiments of Poll (1978) and Arnal (1986) and from the DNS of Spalart (1988) and Joslin (1995). Here, the physical mechanism of the subcritical instability is established from a controlled numerical simulation.

With the results of the present investigation, it is proposed that a three-dimensional simulation be attempted for a physical domain including the wing–fuselage junction along with the leading-edge portion of a sweptback wing by using a high-accuracy DNS method.

REFERENCES

ARNAL, D. 1986 Three-dimensional boundary layers: laminar–turbulent transition. *AGARD Rep.* 741.

ARNAL, D., COUSTOLS, R. & JULLIEN, J. 1984 Etude experimentale et thèorique de la transition sur une aile en flèche infinie. *La Rechereche Aerospatiale* **4**, 275–290.

BRINCKMAN, K. W. & WALKER, J. D. A. 2001 Instability in a viscous flow driven by streamwise vortices. *J. Fluid Mech.* **432**, 127–166.

COOKE, J. C. 1950 The boundary layer of a class of infinite yawed cylinders. *Proc. Camb. Phil. Soc.* **46**, 645–648.

CRABTREE, L. F., KUCHEMANN, D. & SOWERBY, L. 1963 Three Dimensional Boundary layers. In *Laminar Boundary Layers* (ed. L. Rosenhead). Clarendon.

DEGANI, A. T., WALKER, J. D. A. & SMITH, F. T. 1998 Unsteady separation past moving surfaces. *J. Fluid Mech.* **375**, 1–38.

DOLIGALSKI, T. L., SMITH, C. R. & WALKER, J. D. A. 1994 Vortex interaction with walls. *Annu. Rev. Fluid Mech.* **26**, 573–616.

GASTER, M. 1965 A simple device for preventing turbulent contamination on swept leading edges. *J. R. Aero. Soc.* **69**, 788–789.

GASTER, M. 1967 On the flow along swept leading edges. *Aero. Q.* **18**, 165–184.

HALL, P. & MALIK, M. R. 1986 On the instability of three-dimensional attachment-line boundary layer: weakly non-linear theory and numerical approach. *J. Fluid Mech.* **163**, 257–282.

HALL, P., MALIK, M. R. & POLL, D. 1984 On the stability of an infinite swept attachment-line boundary layer. *Proc. R. Soc. Lond.* A **395**, 229–245.

HARAS, Z. & TA'ASAN, S. 1994 Finite difference schemes for long time integration *J. Comput. Phys.* **114**, 265–279.

HOLMES, P., LUMLEY, J. L. & BERKOOZ, G. 1996 *Turbulence, Coherent Structures, Dynamical Systems and Symmetry*. Cambridge University Press.

JOSLIN, R. D. 1995 Direct simulation of evolution and control of three-dimensional instabilities in attachment-line boundary layers. *J. Fluid Mech.* **291**, 369–392.

JOSLIN R. D. 1996 Simulation of non-linear instabilities in an attachment-line boundary layer. *Fluid Dyn. Res.* **18**, 81–97.

KOSAMBI, D. D. 1943 Statistics in function spaces. *J. Indian Math. Soc.* **7**, 76–88.

LIM, T. T., SENGUPTA, T. K. & CHATTOPADHYAY, M. 2004 A visual study vortex-induced subcritical instability on a flat plate laminar boundary layer. *Exps. Fluids* **37**, 47–55.

MONIN, A. S. & YAGLOM, A. M. 1971 *Statistical Fluid Mechanics: Mechanics of Turbulence*. The MIT Press, USA.

MORKOVIN, M. V. 1991 Panoramic view of changes in vorticity distribution in transition instabilities and turbulence. In *Boundary Layer Stability and Transition to Turbulence* (ed. D. C. Reda, H. L. Reed & R. Kobayashi). *ASME FED* **114**, 1–12.

OBABKO, A. V. & CASSEL, K. W. 2002 Navier–Stokes solutions of unsteady separation induced by a vortex. *J. Fluid Mech.* **465**, 99–130.

OBRIST, D. & SCHMID, P. J. 2003*a* On the linear stability of swept attachment-line boundary layer flow. Part 1. Spectrum and asymptotic behavior. *J. Fluid Mech.* **493**, 1–29.

OBRIST, D. & SCHMID, P. J. 2003*b* On the linear stability of swept attachment-line boundary layer flow. Part 2. Non-modal effect and receptivity. *J. Fluid Mech.* **493**, 31–58.

PERIDIER, V. J., SMITH, F. T. & WALKER, J. D. A. 1991*a* Vortex-induced boundary-layer separation. Part 1. The unsteady limit problem. $Re \to \infty$. *J. Fluid Mech.* **232**, 99–131.

PERIDIER, V. J., SMITH, F. T. & WALKER, J. D. A. 1991*b* Vortex–induced boundary-layer separation. Part 2. Unsteady interacting boundary-layer Theory. *J. Fluid Mech.* **232**, 133–265.

PFENNINGER, W. & BACON, J. W. 1969 Amplified laminar boundary-layer oscillations and transition at the front attachment-line of a 45° swept flat-nosed wing with and without suction. In *Viscous Drag Reduction*. (ed. C. S. Wells), pp. 85–105. Plenum.

POLL, D. I. A. 1979 Transition in the infinite swept attachment-line boundary-layer. *Aero. Q.* **30**, 607–629.

POLL, D., DANKS, M. & YARDLEY, M. 1996 The effects of suction and blowing on stability and transition at a swept attachment-line. In *Transitional Boundary Layers in Aeronautics* (ed. R. Henkes & J. Van Ingen). Elsevier.

PRANDTL, L. 1946 On boundary layer in three-dimensional flow. *Rep. Aero. Council, London*, **9828**.

RAJAEE, M., KARLSSON, S. K. F. & SIROVICH, L. 1994 Low-dimensional description of free-shear-flow coherent structures and their dynamical behaviour. *J. Fluid Mech.* **258**, 1–29.

ROBINSON, S. K. 1991 Coherent motions in the turbulent boundary layer. *Annu. Rev. Fluid Mech.* **23**, 601–639.

SENGUPTA, T. K., CHATTOPADHYAY, M., WANG, Z. Y. & YEO, K. S. 2002 By-pass mechanism of transition to turbulence. *J. Fluids Struct.* **16**, 15–29.

SENGUPTA, T. K., CHATURVEDI, V., KUMAR, P. & DE, S. 2004 Computation of leading edge contamination. *Comput. Fluids* **33**, 927–951.

SENGUPTA, T. K., DE, S. & SARKAR, S. 2003*a* Vortex- induced instability of an incompressible wall bounded shear layer. *J. Fluid Mech.* **493**, 277–286.

SENGUPTA, T. K., GANERIWAL, G. & DE, S. 2003*a* Analysis of central and upwind compact schemes. *J. Comput. Phys.* **192**, 677–694.

SENGUPTA, T. K., LIM, T. T. & CHATTOPADHYAY, M. 2001 An experimental and theoretical investigation by-pass transition mechanism. Dept. of Aerospace Engineering, IIT Kanpur. Rep. IITK/Aero/AD/2001/02.

SIROVICH, L. 1987 Turbulence and the dynamics of coherent structures. Part 1–3: Coherent Structures. *Q. Appl. Maths* **45**, 561–584.

SMITH, C. R., WALKER, J. D. A., HAIDARI, A. H. & SOBRUN, U. 1991 On the dynamics of near-wall turbulence. *Phil. Trans. R. Soc. Lond.* A **336**, 131–175.

SPALART, P. R. 1988 Direct numerical study of leading edge contamination. *AGARD CP* **438**, 5.1–5.13.

TAYLOR, G. I. 1936 Statistical theory of turbulence. V. Effect of turbulence on boundary layer. *Proc. Roy. Soc.* A **156**, 307–317.

THEOFILIS, V. 1998 On linear and non-linear instability of the incompressible swept attachment line boundary layer. *J. Fluid Mech.* **355**, 193–227.

THEOFILIS, V., FEDOROV, A., OBRIST, D. & DALLMANN, U. C. 2003 The extended Görtler–Hämmerlin model for linear instability of three-dimensional incompressible swept attachment-line boundary layer flow. *J. Fluid Mech.* **487**, 271–313.